International Journal of Solids and Structures 50 (2013) 4000–4009

Contents lists available at ScienceDirect

International Journal of Solids and Structures

journal homepage: www.elsevier.com/locate/ijsolstr

The extended Durbin method and its application for piezoelectric wave propagation problems

Yi-Shyong Ing *, Hsueh-Fen Liao, Kuo-Shu Huang

Department of Aerospace Engineering, Tamkang University, New Taipei City 25137, Taiwan, ROC

ARTICLE INFO

Article history:
Received 15 March 2013
Received in revised form 24 July 2013
Available online 12 August 2013

Keywords:
Wave propagation
Transient
Piezoelectric
Layered medium
Durbin method
Inversion

ABSTRACT

Based on the well-known Durbin method, an efficient numerical method was developed for the inversion of the two-sided Laplace transform. The accuracy of the method was verified using examples. As an application of the method, transient elastic waves propagating in a two-layered piezoelectric medium subjected to anti-plane concentrated loading and in-plane electric displacement loading were investigated. One-sided and two-sided Laplace transforms were applied to determine the shear stresses and electric displacements in the double Laplace transform domain. Subsequently, the Durbin method for one-sided Laplace transform inversion and the extended Durbin method for two-sided Laplace transform inversion were used to implement the numerical inversions. Additionally, the numerical results of the transient stresses and electric displacements were evaluated and discussed. It showed that the arrival time of transient waves satisfies physical phenomena, and the transient solution oscillates near the static solution and rapidly approximates the static solution.

1. Introduction

With the recent development of materials and advances in manufacturing technology, piezoelectric materials are becoming increasingly common. They are finding new applications in non-destructive evaluation, ultrasonic medical imaging, smart structures, and active control of sound and vibration. In this endeavor, composite materials, consisting of combinations of two or more different piezoelectric and non-piezoelectric material phases, have been designed to meet specific technical needs (Ma et al., 2007). However, most currently available piezoelectric materials are constructed from brittle substances and thus, are prone to brittle fractures when employed in areas of vibration. Therefore, research concerning piezoelectric structural damage is essential.

A systematic methodology for the solution of the multilayered problem was presented by Thomson (1950) and Haskell (1953). They developed the "transfer matrix method" to determine the dispersive characteristics of seismic waves within the Earth modeled by an isotropic multilayered medium. Later, Gilbert and Backus (1966) proposed the propagator matrix method and gave a more formal mathematical interpretation to the technique. Kundu and Mal (1985) applied a modified version of Thomson–Haskell matrix method to the evaluation of the wave motion produced in a multilayered solid by dynamic sources. This modified approach does not suffer from the precision problem and is thus applicable to calculations for all frequency ranges and source-receiver separations. With the development of the direct method of evaluation of integral representations for transient waves in a layered medium (Cagniard, 1962) and the introduction of the concept of generalized ray paths (Spencer, 1960, 1965a,b), the generalized ray theory was adopted (Müller, 1968a,b; Pao and Gajewski, 1977) for analyzing the transient response of a multilayered solid. Recently, Ma and Huang (1996) derived the transfer relation as a general representation of the responses between each layer, instead of the displacement-traction vector, to determine the transient wave propagating in a multilayered medium. Theoretical, numerical, and experimental results for transient responses of a layered medium subject to in-plane loads were presented by Ma and Lee (2000). The dynamic response of a layered medium subject to anti-plane loads was investigated by Ma et al. (2001). Zhuang et al. (2003) conducted an experiment on the influence of scattering effects induced by internal interfaces on shock wave propagation in heterogeneous media. An analytical solution to the problem of plate impact in layered heterogeneous material systems has been developed by Chen et al. (2004). Ma and Lee (2006) investigated the general three-dimensional analysis of transient elastic waves in a multilayered medium.

Many smart structures such as piezoelectric composites are made up of two or more different constituents periodically arranged. The investigation of acoustic waves in piezoelectric phononic crystals has recently attracted much attention (Sesion et al., 2007; Wang et al., 2008; Piliposian et al., 2012). In addition, investigations of transient waves in layered piezoelectric media

* Corresponding author. Tel.: +886 2 26215656x2771; fax: +886 2 26209746.
E-mail address: ysing@mail.tku.edu.tw (Y.-S. Ing).

0020-7683/$ - see front matter © 2013 Elsevier Ltd. All rights reserved.
http://dx.doi.org/10.1016/j.ijsolstr.2013.08.009

were made by Minagawa (1995), Mesquida et al. (1998), Tressler et al. (1999), Qian et al. (2004), Zakharenko (2005), Ma et al. (2007), and Liu and He (2010). The results on the transient waves obtained in numerous studies have shown no significant peaks when arriving at the major transient wave, indicating that the integral calculation or inversion results may possess partial errors. Thus, identifying how to determine precise numerical results is a crucial issue that must be resolved.

Numerous researchers have used the Laplace transform and the inversion of Laplace transform as the primary tools for analyzing dynamic fractures in piezoelectric materials. However, using the analytical inversion of Laplace transform for analysis renders the mathematical composition excessively complex and difficult; therefore, it is only suitable for relatively simple geometric structures. The numerical inversion of Laplace transform is more practical for calculating complex problems. Over 20 numerical methods for inverting the Laplace transform have been proposed in literature, and their application principles differ from each other. For example, the Gaussian quadrature has been used as a foundation for the numerical inversion of Laplace transform (Schmittroth, 1960), as have methods derived from orthogonal functions (Bellman et al., 1966; Miller and Guy, 1966; Week, 1966). Numerous studies have explored the numerical Laplace transform inversion obtained using the Fourier series (Dubner and Abate, 1968; Durbin, 1974; Crump, 1976; Albrecht and Honig, 1977; Honig and Hirdes, 1984). Additionally, many crucial studies and reviews regarding the numerical inversion of Laplace transform have been conducted (Zakian and Coleman, 1971; Singhal et al., 1975; Hosono, 1981; Therapos and Diamessis, 1982; Shih et al., 1987; Kwok and Barthez 1989; Evans, 1993; Wu et al., 2001; Abate and Valkó, 2004; Zhao, 2004; Milovanović and Cvetković, 2005). Although many methods for achieving the numerical inversion of Laplace transform exist, Narayanan and Beskos (1982) applied 8 numerical inversions of Laplace transform to linear dynamic problems, and systematically discussed and calculated their efficiency. Their results showed that the Durbin method (1974) was the best. The Durbin method can provide reliable long-term and short-term results in most cases; however, a comparatively longer calculation time is required.

In studies that analyzed the transient response of piezoelectric materials under dynamic loading, the governing equations are partial differential equations with multiple variables. Therefore, the Laplace transform (referred to as the one-sided Laplace transform in this study) was commonly applied to the time variable when solving partial differential equations, and the Fourier transform was commonly applied to space variables. However, to achieve convenience for various wave propagation problems, the two-sided Laplace transform is often used for space variables. Nevertheless, simultaneously achieving an analytical inversion for one-sided and two-sided Laplace transforms is extremely difficult. Methods similar to the Cagniard method (1939) can only be applied to a few simple problems for analytical inversion; therefore, most problems should be solved using numerical inversion. The accurate and rapid calculation of two inversions is crucial for calculating two-dimensional transient wave propagation. Adopting the Durbin method as the theoretical basis of this study, we inferred the inversion formula for the two-sided Laplace transform (called the extended Durbin method in this study) and employed a few simple functions as examples for calculation to verify the accuracy of this method.

In addition, we also employed the extended Durbin method to examine the two-dimensional transient wave propagation problems of a two-layered piezoelectric medium under anti-plane concentrated and in-plane electric displacement loads. We conducted a detailed calculation and discussed the transient response of the stress and electric displacement fields. The extended Durbin method can be applied to obtain precise numerical results not only on piezoelectric problems, but also on purely-elastic material problems. The present results can degenerate correctly into the case of both layers made of homogeneous purely-elastic materials. Furthermore, we calculated the various parameters of the one-sided and two-sided Laplace inversions, providing superior recommended values as an excellent reference for mutilayered media or in-plane studies in the future.

2. The extended Durbin method

2.1. The Durbin method

Let $f_1(t)$ be a function of time t, with $f_1(t) = 0$ for $t < 0$. The one-sided Laplace transform pair is defined as

$$\bar{f}_1(s) = \int_0^\infty e^{-st} f_1(t)\,dt, \tag{1}$$

$$f_1(t) = \frac{1}{2\pi i}\int_{c_1-i\infty}^{c_1+i\infty} e^{st}\bar{f}_1(s)\,ds, \tag{2}$$

where s is the complex transform parameter, c_1 is a positive constant, and i is the imaginary unit. Durbin (1974) determined the approximation formula shown below:

$$f_1(t) = \frac{2e^{\alpha t}}{T_t}\left\{-\frac{1}{2}\mathrm{Re}[\bar{f}_1(\alpha)] + \sum_{k=0}^{\infty}\left(\mathrm{Re}\left[\bar{f}_1\left(\alpha + i\frac{2k\pi}{T_t}\right)\right]\cos\left(\frac{2\pi kt}{T_t}\right) - \mathrm{Im}\left[\bar{f}_1\left(\alpha + i\frac{2k\pi}{T_t}\right)\right]\sin\left(\frac{2\pi kt}{T_t}\right)\right)\right\}, \tag{3}$$

for $0 \leqslant t \leqslant T_t$. Generally, T_t is considered the inversion duration, and $\alpha T_t = 5$ to 10.

2.2. The extended Durbin method

Let $f_2(x)$ be a function of the space variable x. The two-sided Laplace transform pair is defined as

$$f_2^*(\eta) = \int_{-\infty}^{\infty} e^{-\eta x} f_2(x)\,dx, \tag{4}$$

$$f_2(x) = \frac{1}{2\pi i}\int_{c_2-i\infty}^{c_2+i\infty} e^{\eta x} f_2^*(\eta)\,d\eta, \tag{5}$$

where η is the complex transform parameter, and c_2 is a positive constant.

Let

$$\eta = \beta + i\varpi, \tag{6}$$

to obtain

$$e^{\eta x} = e^{\beta x}(\cos\varpi x + i\sin\varpi x). \tag{7}$$

The transformed function f_2^* can be rewritten as

$$f_2^*(\eta) = \mathrm{Re}[f_2^*(\beta + i\varpi)] + i\,\mathrm{Im}[f_2^*(\beta + i\varpi)]. \tag{8}$$

Thus, (5) has the following form:

$$f_2(x) = \frac{e^{\beta x}}{\pi} \times \int_0^\infty \{\mathrm{Re}[f_2^*(\beta + i\varpi)]\cos\varpi x - \mathrm{Im}[f_2^*(\beta + i\varpi)]\sin\varpi x\}\,d\varpi. \tag{9}$$

The function $f_2(x)$ does not necessarily have to be a symmetrical function, but it must be an exponential-order function as $x \to \infty$ and $x \to -\infty$.

Assume a convergent function,

$$h(x) = f_2(x)e^{-\beta x}. \tag{10}$$

For $0 \leqslant x < \infty$, consider sections of $h(x)$ in intervals similar to $(nT_x, (n+1)T_x)$, and construct an infinite set of $2T_x$-periodic functions $g_n(x)$:

$$g_n(x) = \begin{cases} h(x), & nT_x \leqslant x \leqslant (n+1)T_x, \\ h(2nT_x - x), & (n-1)T_x \leqslant x \leqslant nT_x, \end{cases} \quad n = 0,1,2,\ldots, \quad 0 \leqslant x < \infty. \tag{11}$$

Based on the Fourier cosine series expansion (Dubner and Abate, 1968), we obtain

$$\sum_{n=0}^{\infty} e^{\beta x} g_n(x) = \frac{2e^{\beta x}}{T_x}\left\{\frac{1}{2}A_1(\varpi_0) + \sum_{k=1}^{\infty} A_1(\varpi_k)\cos\left(\frac{k\pi x}{T_x}\right)\right\}, \quad 0 \leqslant x < \infty, \tag{12}$$

where

$$A_1(\varpi_k) = \int_0^{\infty} e^{-\beta x} f_2(x)\cos\left(\frac{k\pi x}{T_x}\right)dx. \tag{13}$$

For $-\infty < x < 0$, introduce a new function:

$$g_n(x) = \begin{cases} h(x), & -(n+1)T_x \leqslant x \leqslant -nT_x, \\ h(-2nT_x - x), & -nT_x \leqslant x \leqslant -(n-1)T_x, \end{cases} \quad n = 0,1,2,\ldots, \quad -\infty < x < 0. \tag{14}$$

Developing each $g_n(x)$ into a Fourier cosine series, we obtain a relationship similar to that of (12):

$$\sum_{n=0}^{\infty} e^{\beta x} g_n(x) = \frac{2e^{\beta x}}{T_x}\left\{\frac{1}{2}A_2(\varpi_0) + \sum_{k=1}^{\infty} A_2(\varpi_k)\cos\left(\frac{k\pi x}{T_x}\right)\right\}, \quad -\infty < x < 0, \tag{15}$$

where

$$A_2(\varpi_k) = \int_{-\infty}^{0} e^{-\beta x} f_2(x)\cos\left(\frac{k\pi x}{T_x}\right)dx. \tag{16}$$

Based on (12) and (15), the formula for inverting the two-sided Laplace transform using the approach employed by Dubner and Abate (1968) can be expressed as follows:

$$f_2(x) = \frac{2e^{\beta x}}{T_x}\left\{\frac{1}{2}\mathrm{Re}[f_2^*(\beta)] + \sum_{k=1}^{\infty}\mathrm{Re}\left[f_2^*\left(\beta + i\frac{k\pi}{T_x}\right)\right]\cos\left(\frac{k\pi x}{T_x}\right)\right\}, \quad -\infty < x < \infty. \tag{17}$$

Similarly, if we construct an infinite set of odd $2T_x$-periodic functions $k_n(x)$ (Durbin, 1974) and develop each $k_n(x)$ into a Fourier sine series, another representation of $f_2(x)$ can be expressed as follows:

$$f_2(x) = -\frac{2e^{\beta x}}{T_x}\sum_{k=0}^{\infty}\mathrm{Im}\left[f_2^*\left(\beta + i\frac{k\pi}{T_x}\right)\right]\sin\left(\frac{k\pi x}{T_x}\right), \quad -\infty < x < \infty. \tag{18}$$

By summing half of both sides of (17) and (18), and changing T_x into $T_x/2$, the approximation formula of the extended Durbin method for the two-sided Laplace transform inversion can be obtained, as shown below:

$$f_2(x) = \frac{2e^{\beta x}}{T_x}\left\{-\frac{1}{2}\mathrm{Re}[f_2^*(\beta)] + \sum_{k=0}^{\infty}\left(\mathrm{Re}\left[f_2^*\left(\beta + i\frac{2k\pi}{T_x}\right)\right]\cos\left(\frac{2\pi kx}{T_x}\right) - \mathrm{Im}\left[f_2^*\left(\beta + i\frac{2k\pi}{T_x}\right)\right]\sin\left(\frac{2\pi kx}{T_x}\right)\right)\right\}, \quad -\infty < x < \infty. \tag{19}$$

Notably, (19) is identical to the Durbin formula (3). This means that the Durbin method for the one-sided Laplace transform inversion can be directly employed for the two-sided Laplace transform inversion. However, we subsequently found that the set values for the related parameters differed significantly between these two cases.

Table 1
Test function 1: $f_2(x) = 2[H(x+2) - H(x-2)] = L^{-1}\{2(e^{2\eta} - e^{-2\eta})/\eta\}$.

x	Exact	Extended Dubrin's method	Error %
−2.2	0.000000000	−0.001697408	–
−2.0	2.000000000	0.999987028	−50.0006
−1.8	2.000000000	2.001692662	0.0846
−1.6	2.000000000	2.000546850	0.0273
−1.4	2.000000000	1.999019177	−0.0490
−1.2	2.000000000	2.000579804	0.0290
−1.0	2.000000000	2.000052541	0.0026
−0.8	2.000000000	1.999546119	−0.0227
−0.6	2.000000000	2.000439091	0.0220
−0.4	2.000000000	1.999885568	−0.0057
−0.2	2.000000000	1.999746541	−0.0127
−0.0	2.000000000	2.000409395	0.0205
0.2	2.000000000	1.999747059	−0.0126
0.4	2.000000000	1.999885029	−0.0057
0.6	2.000000000	2.000439131	0.0220
0.8	2.000000000	1.999546616	−0.0227
1.0	2.000000000	2.000051984	0.0026
1.2	2.000000000	2.000579885	0.0290
1.4	2.000000000	1.999019653	−0.0490
1.6	2.000000000	2.000546277	0.0273
1.8	2.000000000	2.001692783	0.0846
2.0	2.000000000	0.999987477	−50.0006
2.2	0.000000000	−0.001697997	–

2.3. Examples

Two examples are tested below.
Function 1:

$$f_2^*(\eta) = \int_{-\infty}^{\infty} e^{-\eta x}\cdot 2[H(x+2) - H(x-2)]dx = 2(e^{2\eta} - e^{-2\eta})/\eta. \tag{20}$$

Function 2:

$$f_2^*(\eta) = \int_{-\infty}^{\infty} e^{-\eta x}\cdot\cos(x)[H(x+5) - H(x-10)]dx = [e^{-10\eta}(\sin 10 - \eta\cos 10) + e^{5\eta}(\sin 5 + \eta\cos 5)]/(\eta^2+1), \tag{21}$$

where $H()$ is the Heaviside function.

The parameters were set as $\beta T_x = 0.01$, $T_x = 30$, and $N = 5000$. The results are shown in Tables 1 and 2. The results show that the values obtained using the extended Durbin method agree well with the actual values. Significantly, for these two functions, which possess discontinuity at $x = x_0$, the extended Durbin method provides a numerical value that is extremely similar to the theoretical value, $[f_2(x_0+) + f_2(x_0-)]/2$. Theoretically, the larger the total number of summations N, the more accurate the inversion. However, considerable computations are required, which is time-consuming when solving transient wave problems.

3. Application in the transient response of a piezoelectric laminate

3.1. Statement of the problem

The specific geometry considered in this study was a two-layered piezoelectric laminate with a perfectly bonded interface. The thickness of the upper and lower layers were h_1 and h_2, respectively. For $t < 0$, the composite was stress free and at rest. At time $t = 0$, a pair of dynamic anti-plane concentrated forces P and

Table 2
Test function 2: $f_2(x) = cos(x)[H(x+5) - H(x-10)] = L^{-1}\{[e^{-10\eta}(sin\,10 - \eta cos\,10) + e^{5\eta}(sin\,5 + \eta cos\,5)/(\eta^2+1)\}]$.

x	Exact	Extended Dubrin's method	Error %
−11	0.000000000	−0.000006800	–
−10	0.000000000	−0.000030999	–
−9	0.000000000	0.000026596	–
−8	0.000000000	0.000019097	–
−7	0.000000000	−0.000049256	–
−6	0.000000000	−0.000010795	–
−5	0.283662185	0.141539740	−50.1027
−4	−0.653643621	−0.653632778	−0.0017
−3	−0.989992497	−0.989943229	−0.0050
−2	−0.416146837	−0.416166040	0.0046
−1	0.540302306	0.540275604	−0.0049
0	1.000000000	1.000030902	0.0031
1	0.540302306	0.540309271	0.0013
2	−0.416146837	−0.416184082	0.0089
3	−0.989992497	−0.989972421	−0.0020
4	−0.653643621	−0.653613609	−0.0046
5	0.283662185	0.283610628	−0.0182
6	0.960170287	0.960173180	0.0003
7	0.753902254	0.753981689	0.0105
8	−0.145500034	−0.145592610	0.0636
9	−0.911130262	−0.911226479	0.0106
10	−0.839071529	−0.419700803	−49.9803
11	0.000000000	0.000095317	–

electric charges D_0 act at the upper and lower free surfaces, as shown in Fig. 1. The piezoelectric layer is poled in the z-direction exhibiting transversely isotropic behavior. Assuming that only the out-of-plane displacement and the in-plane electric fields are considered. The dynamic anti-plane governing equations can be expressed as

$$c_{44}^{(j)}\nabla^2 w_j + e_{15}^{(j)}\nabla^2\phi_j = \rho^{(j)}\ddot{w}_j, \quad (j=1,2), \tag{22}$$

$$e_{15}^{(j)}\nabla^2 w_j - \varepsilon_{11}^{(j)}\nabla^2\phi_j = 0, \quad (j=1,2), \tag{23}$$

where $w_j = w_j(x,y)$ is the anti-plane displacement in the z-direction (which is assumed to align with the symmetry axis), $\phi_j = \phi_j(x,y)$ is the electric potential, $c_{44}^{(j)}$ is the elastic modulus measured in a constant electric field, $\varepsilon_{11}^{(j)}$ is the dielectric permittivity measured at a constant strain, $e_{15}^{(j)}$ is the piezoelectric constant, and $\rho^{(j)}$ is the material density. The superscript or subscript $j = 1$ represents the quantities related to the upper layer (piezoelectric material 1), and $j = 2$ represents those of the lower layer (piezoelectric material 2). $\nabla^2 = \partial^2/\partial x^2 + \partial^2/\partial y^2$ is the in-plane Laplacian, and a dot denotes the material time derivative.

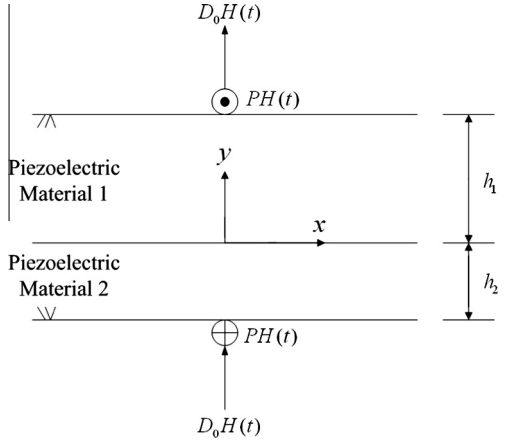

Fig. 1. Configuration and coordinate systems of a two-layered piezoelectric medium subjected to mechanical and electric impacts.

The constitutive equations for the piezoelectric composite can be expressed as

$$\tau_{yz}^{(j)} = c_{44}^{(j)}\frac{\partial w_j}{\partial y} + e_{15}^{(j)}\frac{\partial \phi_j}{\partial y} \quad (j=1,2), \tag{24}$$

$$\tau_{xz}^{(j)} = c_{44}^{(j)}\frac{\partial w_j}{\partial x} + e_{15}^{(j)}\frac{\partial \phi_j}{\partial x} \quad (j=1,2), \tag{25}$$

$$D_y^{(j)} = e_{15}^{(j)}\frac{\partial w_j}{\partial y} - \varepsilon_{11}^{(j)}\frac{\partial \phi_j}{\partial y} \quad (j=1,2), \tag{26}$$

$$D_x^{(j)} = e_{15}^{(j)}\frac{\partial w_j}{\partial x} - \varepsilon_{11}^{(j)}\frac{\partial \phi_j}{\partial x} \quad (j=1,2), \tag{27}$$

where $\tau_{yz}^{(j)}$ and $\tau_{xz}^{(j)}$ are shear stresses, and $D_y^{(j)}$ and $D_x^{(j)}$ are electric displacements.

The boundary conditions of this problem can be expressed as

$$\tau_{yz}^{(1)}(x,h_1,t) = P\delta(x)H(t), \quad -\infty < x < \infty, \tag{28}$$

$$D_y^{(1)}(x,h_1,t) = D_0\delta(x)H(t), \quad -\infty < x < \infty, \tag{29}$$

$$w_1(x,0,t) = w_2(x,0,t), \quad -\infty < x < \infty, \tag{30}$$

$$\tau_{yz}^{(1)}(x,0,t) = \tau_{yz}^{(2)}(x,0,t), \quad -\infty < x < \infty, \tag{31}$$

$$\phi_1(x,0,t) = \phi_2(x,0,t), \quad -\infty < x < \infty, \tag{32}$$

$$D_y^{(1)}(x,0,t) = D_y^{(2)}(x,0,t), \quad -\infty < x < \infty, \tag{33}$$

$$\tau_{yz}^{(2)}(x,-h_2,t) = P\delta(x)H(t), \quad -\infty < x < \infty, \tag{34}$$

$$D_y^{(2)}(x,-h_2,t) = D_0\delta(x)H(t), \quad -\infty < x < \infty, \tag{35}$$

where $\delta(x)$ is the Dirac delta function.

Introducing function $\psi_j = \phi_j - (e_{15}^{(j)}w_j/\varepsilon_{11}^{(j)})$, the solutions of (22) and (23) can be obtained from the following two uncoupled equations:

$$\nabla^2 w_j(x,y,t) = \frac{\rho^{(j)}}{\tilde{c}_{44}^{(j)}}\ddot{w}_j(x,y,t) \quad (j=1,2), \tag{36}$$

$$\nabla^2 \psi_j(x,y,t) = 0 \quad (j=1,2), \tag{37}$$

where $\tilde{c}_{44}^{(j)} = c_{44}^{(j)} + e_{15}^{(j)2}/\varepsilon_{11}^{(j)}$ is the piezoelectrically stiffened elastic constant. Thus, the constitutive equations are reduced to the following forms:

$$\tau_{yz}^{(j)}(x,y,t) = \tilde{c}_{44}^{(j)}\frac{\partial w_j(x,y,t)}{\partial y} + e_{15}^{(j)}\frac{\partial \psi_j(x,y,t)}{\partial y} \quad (j=1,2), \tag{38}$$

$$\tau_{xz}^{(j)}(x,y,t) = \tilde{c}_{44}^{(j)}\frac{\partial w_j(x,y,t)}{\partial x} + e_{15}^{(j)}\frac{\partial \psi_j(x,y,t)}{\partial x} \quad (j=1,2), \tag{39}$$

$$D_y^{(j)}(x,y,t) = -\varepsilon_{11}^{(j)}\frac{\partial \psi_j(x,y,t)}{\partial y} \quad (j=1,2), \tag{40}$$

$$D_x^{(j)}(x,y,t) = -\varepsilon_{11}^{(j)}\frac{\partial \psi_j(x,y,t)}{\partial x} \quad (j=1,2). \tag{41}$$

3.2. Solutions in the Laplace transform domain

When analyzing transient wave problems, the two-sided Laplace transform pair in (4) and (5) can be conveniently expressed as

$$f_2^*(\lambda) = \int_{-\infty}^{\infty} e^{-s\lambda x} f_2(x) dx, \tag{42}$$

$$f_2(x) = \frac{s}{2\pi i} \int_{c_2/s-i\infty}^{c_2/s+i\infty} e^{s\lambda x} f_2^*(\lambda) d\lambda. \tag{43}$$

Here, we let $\eta = s\lambda$ in (4) and (5), and s is the parameter of the one-sided Laplace transform.

Applying (1), (2), (42), and (43) to the uncoupled governing equations, (36) and (37) can be represented as

$$\frac{d^2 \bar{w}_j^*(\lambda, y, s)}{dy^2} - (b_j^2 - \lambda^2) s^2 \bar{w}_j^*(\lambda, y, s) = 0 \quad (j = 1, 2), \tag{44}$$

$$\frac{d^2 \bar{\psi}_j^*(\lambda, y, s)}{dy^2} - \left(\varepsilon^{(j)^2} - \lambda^2\right) s^2 \bar{\psi}_j^*(\lambda, y, s) = 0 \quad (j = 1, 2), \tag{45}$$

where $b_j = \sqrt{\rho^{(j)}/\tilde{c}_{44}^{(j)}}$ is the slowness of the bulk shear horizontal (SH) wave in the piezoelectric material. $\varepsilon^{(j)} \to 0^+$ is an auxiliary positive real perturbation parameter.

The general solutions to (44) and (45) in the double transformed domain have the following form:

$$\bar{w}_j^*(\lambda, y, s) = A_1^{(j)}(\lambda, s) e^{s\alpha^{(j)} y} + A_2^{(j)}(\lambda, s) e^{-s\alpha^{(j)} y} \quad (j = 1, 2), \tag{46}$$

$$\bar{\psi}_j^*(\lambda, y, s) = A_3^{(j)}(\lambda, s) e^{-s\beta^{(j)} y} + A_4^{(j)}(\lambda, s) e^{s\beta^{(j)} y} \quad (j = 1, 2), \tag{47}$$

where $A_1^{(j)}$, $A_2^{(j)}$, $A_3^{(j)}$, and $A_4^{(j)}$ are unknown functions. $\alpha^{(j)} = \sqrt{b_j^2 - \lambda^2}$ for $\mathrm{Re}(\alpha) > 0$, and $\beta^{(j)}(\lambda) = \lim_{\varepsilon^{(j)} \to 0^+} \sqrt{\varepsilon^{(j)^2} - \lambda^2}$.

The 8 undetermined functions can be resolved accurately using the 8 boundary conditions. The process is complicated and tricky, and therefore the detailed derivation is omitted. By applying the one-sided Laplace transform over time t and the two-sided Laplace transform to the spatial variable x for the boundary conditions (28)–(35), with the assistance of (38)–(41), the unknown coefficients $A_1^{(2)}$ and $A_3^{(1)}$ can be obtained as follows:

$$U = \frac{(1+\kappa_2^2)\left(e_{15}^{(1)}\varepsilon_{11}^{(2)} - e_{15}^{(2)}\varepsilon_{11}^{(1)}\right)}{\varepsilon_{11}^{(1)}\varepsilon_{11}^{(2)}}, \tag{52}$$

$$G = (1+\kappa_1^2)(\kappa_4^2 - 1)\varepsilon^{(2)}\beta^{(2)} - (1-\kappa_3^2)(\kappa_4^2 + 1)\varepsilon^{(1)}\beta^{(1)}, \tag{53}$$

$$W = \frac{GZ + \beta^{(1)}\beta^{(2)}\left(e_{15}^{(1)}\varepsilon_{11}^{(2)} - e_{15}^{(2)}\varepsilon_{11}^{(1)}\right)(1-\kappa_3^2)(\kappa_1^2+1)(\kappa_4^2-1)U}{\varepsilon_{11}^{(2)}\beta^{(2)}(\kappa_4^2-1)Z}, \tag{54}$$

$$Q = \frac{\left(e_{15}^{(1)}\varepsilon_{11}^{(2)} - e_{15}^{(2)}\varepsilon_{11}^{(1)}\right)\beta^{(1)}(1-\kappa_3^2)(\kappa_1^2+1)}{\varepsilon_{11}^{(2)}Z}. \tag{55}$$

From the boundary conditions Eqs. (28)–(30), (33)–(35), the remaining 6 unknown functions can be determined using

$$A_2^{(1)} = -\frac{\left(P\varepsilon_{11}^{(2)} + D_0 e_{15}^{(2)}\right)\kappa_2}{s^2\varepsilon_{11}^{(2)}\tilde{c}_{44}^{(2)}\alpha^{(2)}(\kappa_1^2+1)} - \frac{\left(P\varepsilon_{11}^{(1)} + D_0 e_{15}^{(1)}\right)\kappa_1}{s^2\varepsilon_{11}^{(1)}\tilde{c}_{44}^{(1)}\alpha^{(1)}(\kappa_1^2+1)} + \frac{(1+\kappa_2^2)}{(\kappa_1^2+1)}A_1^{(2)}, \tag{56}$$

$$A_2^{(2)} = \frac{-\left(P\varepsilon_{11}^{(2)} + D_0 e_{15}^{(2)}\right)\kappa_2}{s^2\varepsilon_{11}^{(2)}\tilde{c}_{44}^{(2)}\alpha^{(2)}} + \kappa_2^2 A_1^{(2)}, \tag{57}$$

$$A_1^{(1)} = \frac{\left(P\varepsilon_{11}^{(1)} + D_0 e_{15}^{(1)}\right)\kappa_1}{s^2\varepsilon_{11}^{(1)}\tilde{c}_{44}^{(1)}\alpha^{(1)}} + \kappa_1^2 A_2^{(1)}, \tag{58}$$

$$A_4^{(1)} = -\frac{D_0\kappa_3}{s^2\varepsilon_{11}^{(1)}\beta^{(1)}} + \kappa_3^2 A_3^{(1)}, \tag{59}$$

$$A_4^{(2)} = \frac{D_0(\kappa_3 - \kappa_4)}{s^2\varepsilon_{11}^{(2)}\beta^{(2)}(\kappa_4^2-1)} + A_3^{(1)}\frac{\varepsilon_{11}^{(1)}\beta^{(1)}(1-\kappa_3^2)}{\varepsilon_{11}^{(2)}\beta^{(2)}(\kappa_4^2-1)}, \tag{60}$$

$$\begin{aligned} A_1^{(2)} = {} & \frac{D_0 e_{15}^{(1)}\kappa_3(\kappa_1^2+1) - 2\kappa_1\left(P\varepsilon_{11}^{(1)} + D_0 e_{15}^{(1)}\right)}{s^2\varepsilon_{11}^{(1)}Z} + \frac{\left(P\varepsilon_{11}^{(2)} + D_0 e_{15}^{(2)}\right)\kappa_2(\kappa_1^2-1)\left(\tilde{c}_{44}^{(1)}\alpha^{(1)} + \tilde{c}_{44}^{(2)}\alpha^{(2)}\right) - D_0 e_{15}^{(2)}\kappa_3(\kappa_1^2+1)\tilde{c}_{44}^{(2)}\alpha^{(2)}}{s^2\varepsilon_{11}^{(2)}\tilde{c}_{44}^{(2)}\alpha^{(2)}Z} + \frac{D_0\kappa_3 Q}{s^2\varepsilon_{11}^{(1)}\beta^{(1)}W} \\ & + \frac{D_0\left[\kappa_3(\kappa_4^2+1) - 2\kappa_4\right]Q}{s^2\varepsilon_{11}^{(2)}\beta^{(2)}(\kappa_4^2-1)W} - \frac{\left[D_0 e_{15}^{(1)}\kappa_3(\kappa_1^2+1) - 2\kappa_1\left(P\varepsilon_{11}^{(1)} + D_0 e_{15}^{(1)}\right)\right]UQ}{s^2\varepsilon_{11}^{(1)}ZW} \\ & - \frac{\left[\left(P\varepsilon_{11}^{(2)} + D_0 e_{15}^{(2)}\right)\kappa_2(\kappa_1^2-1)\left(\tilde{c}_{44}^{(1)}\alpha^{(1)} + \tilde{c}_{44}^{(2)}\alpha^{(2)}\right) - D_0 e_{15}^{(2)}\kappa_3(\kappa_1^2+1)\tilde{c}_{44}^{(2)}\alpha^{(2)}\right]UQ}{s^2\varepsilon_{11}^{(2)}\tilde{c}_{44}^{(2)}\alpha^{(2)}ZW} + \frac{\left(P\varepsilon_{11}^{(2)} + D_0 e_{15}^{(2)}\right)\kappa_2\left(e_{15}^{(1)}\varepsilon_{11}^{(2)} - e_{15}^{(2)}\varepsilon_{11}^{(1)}\right)Q}{s^2\varepsilon_{11}^{(1)}\varepsilon_{11}^{(2)2}\tilde{c}_{44}^{(2)}\alpha^{(2)}W}, \end{aligned} \tag{48}$$

$$\begin{aligned} A_3^{(1)} = {} & \frac{D_0\kappa_3}{s^2\varepsilon_{11}^{(1)}\beta^{(1)}W} + \frac{D_0\left[\kappa_3(\kappa_4^2+1) - 2\kappa_4\right]}{s^2\varepsilon_{11}^{(2)}\beta^{(2)}(\kappa_4^2-1)W} - \frac{\left[D_0 e_{15}^{(1)}\kappa_3(\kappa_1^2+1) - 2\kappa_1\left(P\varepsilon_{11}^{(1)} + D_0 e_{15}^{(1)}\right)\right]U}{s^2\varepsilon_{11}^{(1)}ZW} \\ & - \frac{\left[\left(P\varepsilon_{11}^{(2)} + D_0 e_{15}^{(2)}\right)(\kappa_1^2-1)\kappa_2\left(\tilde{c}_{44}^{(1)}\alpha^{(1)} + \tilde{c}_{44}^{(2)}\alpha^{(2)}\right) - D_0 e_{15}^{(2)}\kappa_3(\kappa_1^2+1)\tilde{c}_{44}^{(2)}\alpha^{(2)}\right]U}{s^2\varepsilon_{11}^{(2)}\tilde{c}_{44}^{(2)}\alpha^{(2)}ZW} + \frac{\left(P\varepsilon_{11}^{(2)} + D_0 e_{15}^{(2)}\right)\kappa_2\left(e_{15}^{(1)}\varepsilon_{11}^{(2)} - e_{15}^{(2)}\varepsilon_{11}^{(1)}\right)}{s^2\varepsilon_{11}^{(1)}\varepsilon_{11}^{(2)2}\tilde{c}_{44}^{(2)}\alpha^{(2)}W}, \end{aligned} \tag{49}$$

where

$$\kappa_1 = e^{-s\alpha^{(1)}h_1}, \quad \kappa_2 = e^{-s\alpha^{(2)}h_2}, \quad \kappa_3 = e^{-s\beta^{(1)}h_1}, \quad \kappa_4 = e^{-s\beta^{(2)}h_2}, \tag{50}$$

$$Z = (1+\kappa_2^2)(\kappa_1^2-1)\tilde{c}_{44}^{(1)}\alpha^{(1)} - (1-\kappa_2^2)(\kappa_1^2+1)\tilde{c}_{44}^{(2)}\alpha^{(2)}, \tag{51}$$

$$A_3^{(2)} = \frac{D_0\kappa_4}{s^2\varepsilon_{11}^{(2)}\beta^{(2)}} + \kappa_4^2 A_4^{(2)}. \tag{61}$$

Substituting (46) and (47) into the constitutive equations in the double Laplace transform domain, the shear stress $\bar{\tau}_{yz}^{*(j)}$ and electric displacement $\bar{D}_y^{*(j)}$ can be obtained as follows:

$$\bar{\tau}_{yz}^{*(j)}(\lambda,y,s)=\tilde{c}_{44}^{(j)}s\alpha^{(j)}A_1^{(j)}e^{s\alpha^{(j)}y}-\tilde{c}_{44}^{(j)}s\alpha^{(j)}A_2^{(j)}e^{-s\alpha^{(j)}y}-e_{15}^{(j)}s\beta^{(j)}A_3^{(j)}e^{-s\beta^{(j)}y}+e_{15}^{(j)}s\beta^{(j)}A_4^{(j)}e^{s\beta^{(j)}y},\tag{62}$$

$$\bar{D}_y^{*(j)}(\lambda,y,s)=\varepsilon_{11}^{(j)}s\beta^{(j)}A_3^{(j)}e^{-s\beta^{(j)}y}-\varepsilon_{11}^{(j)}s\beta^{(j)}A_4^{(j)}e^{s\beta^{(j)}y}.\tag{63}$$

3.3. Numerical results and discussion

In the previous subsection, the shear stresses and electric displacements in the double Laplace transform domain were derived analytically. To obtain transient solutions, numerical inversions of the one-sided and two-sided Laplace transforms must be performed. Our substantial computational results show that the sequence of the two inversions significantly influences the convergence and accuracy of the transient response. Inversion of the one-sided Laplace transform must be conducted after the two-sided Laplace transform inversion. By substituting (3) into (19), we can obtain the inversion formula as follows:

where

$$P_{31}=\left(e_{15}^{(1)}+e_{15}^{(2)}\right)^2+\left(\tilde{c}_{44}^{(1)}+\tilde{c}_{44}^{(2)}\right)\left(\varepsilon_{11}^{(1)}+\varepsilon_{11}^{(2)}\right),$$

$$P_{33}=e_{15}^{(1)^2}-e_{15}^{(2)^2}+\left(\tilde{c}_{44}^{(1)}+\tilde{c}_{44}^{(2)}\right)\left(\varepsilon_{11}^{(1)}+\varepsilon_{11}^{(2)}\right),$$

$$P_{35}=e_{15}^{(1)}e_{15}^{(2)}+e_{15}^{(2)^2}+\tilde{c}_{44}^{(2)}\left(\varepsilon_{11}^{(1)}+\varepsilon_{11}^{(2)}\right),$$

$$\Theta_3(h,x,y)=\frac{\cosh\left[\frac{\pi}{2h}(x)\right]\sin\left[\frac{\pi}{2h}(y)\right]}{\cosh\left[\frac{\pi}{h}(x)\right]-\cos\left[\frac{\pi}{h}(y)\right]},$$

$$\Theta_4(h,x,y)=\frac{\sin\left[\frac{\pi}{h}(y)\right]}{\cosh\left[\frac{\pi}{h}(x)\right]-\cos\left[\frac{\pi}{h}(y)\right]}.$$

When only a mechanical load was applied to a two-layered piezoelectric strip of equal thickness, Figs. 2 and 3 show a comparison between the transient numerical and static solutions of the shear stress from various observation points. Fig. 2 shows the results of the observation point (0,0) on the interface of the two materials,

$$\begin{aligned}f(t,x)=\frac{2e^{\beta x}}{T_x}\Bigg\{&-\frac{1}{2}\mathrm{Re}\left[\frac{2e^{\alpha t}}{T_t}\left\{-\frac{1}{2}\mathrm{Re}[\bar{f}^*(s,\lambda)|_{s=\alpha}^{\lambda=\beta}]+\sum_{k_1=0}^{N_1}\left\{\mathrm{Re}\left[\bar{f}^*(s,\lambda)|_{s=\alpha+i\frac{k_1 2\pi}{T_t}}^{\lambda=\beta}\right]\cos\left(\frac{k_1 2\pi t}{T_t}\right)-\mathrm{Im}\left[\bar{f}^*(s,\lambda)|_{s=\alpha+i\frac{k_1 2\pi}{T_t}}^{\lambda=\beta}\right]\sin\left(\frac{k_1 2\pi t}{T_t}\right)\right\}\right\}\right]\\&+\sum_{k_3=0}^{N_3}\left\{\mathrm{Re}\left[\frac{2e^{\alpha t}}{T_t}\left\{-\frac{1}{2}\mathrm{Re}\left[\bar{f}^*(s,\lambda)|_{s=\alpha}^{\lambda=\beta+i\frac{k_3 2\pi}{T_x}}\right]+\sum_{k_2=0}^{N_2}\left\{\mathrm{Re}\left[\bar{f}^*(s,\lambda)|_{s=\alpha+i\frac{k_2 2\pi}{T_t}}^{\lambda=\beta+i\frac{k_3 2\pi}{T_x}}\right]\cos\left(\frac{k_2 2\pi t}{T_t}\right)-\mathrm{Im}\left[\bar{f}^*(s,\lambda)|_{s=\alpha+i\frac{k_2 2\pi}{T_t}}^{\lambda=\beta+i\frac{k_3 2\pi}{T_x}}\right]\sin\left(\frac{k_2 2\pi t}{T_t}\right)\right\}\right\}\right]\cos\left(\frac{k_3 2\pi x}{T_x}\right)\\&-\mathrm{Im}\left[\frac{2e^{\alpha t}}{T_t}\left\{-\frac{1}{2}\mathrm{Re}\left[\bar{f}^*(s,\lambda)|_{s=\alpha}^{\lambda=\beta+i\frac{k_3 2\pi}{T_x}}\right]+\sum_{k_2=0}^{N_2}\left\{\mathrm{Re}\left[\bar{f}^*(s,\lambda)|_{s=\alpha+i\frac{k_2 2\pi}{T_t}}^{\lambda=\beta+i\frac{k_3 2\pi}{T_x}}\right]\cos\left(\frac{k_2 2\pi t}{T_t}\right)-\mathrm{Im}\left[\bar{f}^*(s,\lambda)|_{s=\alpha+i\frac{k_2 2\pi}{T_t}}^{\lambda=\beta+i\frac{k_3 2\pi}{T_x}}\right]\sin\left(\frac{k_2 2\pi t}{T_t}\right)\right\}\right]\sin\left(\frac{k_3 2\pi x}{T_x}\right)\right\}\Bigg\}.\end{aligned}\tag{64}$$

The relevant parameter settings during the calculation process were $\alpha T_t=5$, $N_1=1000$, $N_2=3000$, and $N_3=3000$. Following the recommendation by Ing and Liao (2012), the period T_t was twice the maximum value of the calculated time period. Furthermore, we recommend that the setting values of period T_x be divided into two conditions: (I) when the observation point is at the origin (0,0), period T_x is set as 10 and βT_x is set as 0.01; and (II) when the observation point is not at the origin (0,0), period T_x is set between 30 and 50 and βT_x is set as 0.01.

Two transversely isotropic piezoelectric materials, PZT4 and ZnO, were used as the upper and lower layer materials for calculation. The relevant material constants were as follows:

$$c_{44}^{(1)}=2.56\times10^{10}\ \mathrm{N/m^2},\quad e_{15}^{(1)}=12.7\ \mathrm{C/m^2},$$
$$\varepsilon_{11}^{(1)}=64.6\times10^{-10}\ \mathrm{F/m^2},\quad b_1=3.852\times10^{-4}\ \mathrm{s/m},$$

$$c_{44}^{(2)}=4.25\times10^{10}\ \mathrm{N/m^2},\quad e_{15}^{(2)}=-0.48\ \mathrm{C/m^2},$$
$$\varepsilon_{11}^{(2)}=0.757\times10^{-10}\ \mathrm{F/m^2},\quad b_2=3.534\times10^{-4}\ \mathrm{s/m}.$$

First, the transient response for shear stresses in a two-layered piezoelectric strip of equal thickness ($h_1=h_2$) was considered. The static solution proposed by Wang (2003) were compared to verify the accuracy of the results proposed in this study. Employing the solution proposed by Wang (2003) in this problem results in the following static solution:

$$\tau_{yz}(x,y)=\frac{P}{4P_{31}h}\{(P_{31}-P_{33})[2\Theta_3(h,x,-y+h)]+(P_{31}+P_{33})\times[\Theta_4(h,x,-y+h)]+P_{35}[2\Theta_4(2h,x,y+h)]\},\tag{65}$$

and indicates that when the non-dimensional time $t/b_2h_2=1$ and $t/b_2h_2\cong1.09$, the incident bulk SH waves of the upper and lower layer material reach the observation point in succession. Addition-

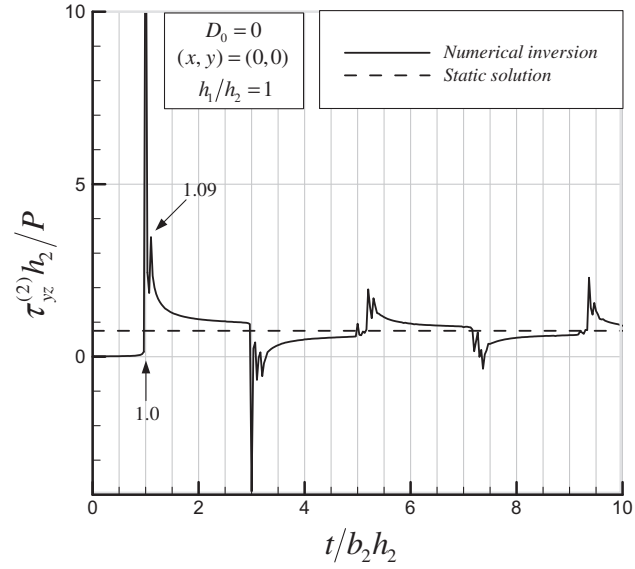

Fig. 2. Normalized transient shear stresses versus normalized time at (0,0) ($N_1=1000$, $N_2=3000$, $N_3=3000$, $h_1/h_2=1$, $T_t=20b_2h_2$, $\alpha T_t=5$, $T_x=10$, $\beta T_x=0.01$).

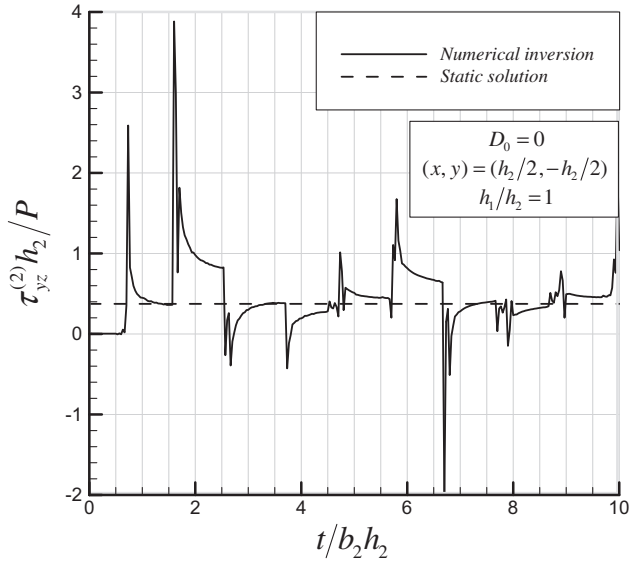

Fig. 3. Normalized transient shear stresses versus normalized time at $(h_2/2, -h_2/2)$ (N_1 = 1000, N_2 = 3000, N_3 = 3000, h_1/h_2 = 1, $T_t = 20b_2h_2$, αT_t = 5, T_x = 30, βT_x = 0.01).

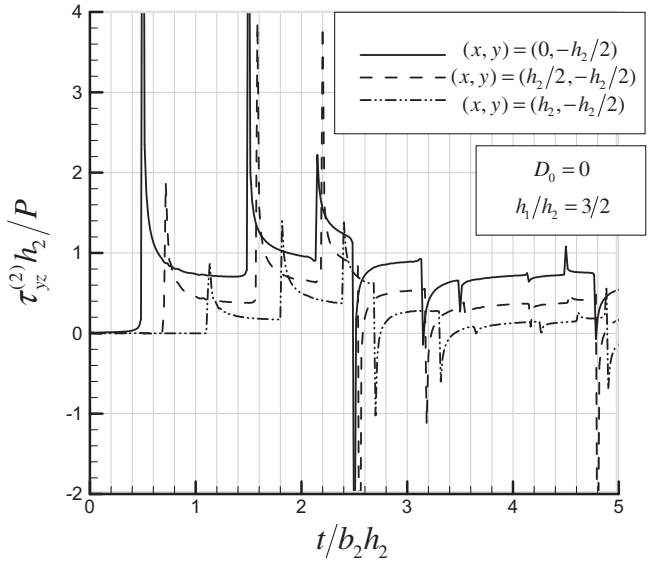

Fig. 5. Normalized transient shear stresses versus normalized time at $y = -h_2/2$ (N_1 = 1000, N_2 = 3000, N_3 = 3000, h_1/h_2 = 3/2, $T_t = 20b_2h_2$, αT_t = 5, T_x = 30, βT_x = 0.01).

ally, when the incident bulk SH wave reaches the observation point, the shear stress approximates infinity because the load applied is a point load. Furthermore, a series of reflected waves successively arrive in a short period following $t/b_2h_2 = 3$ because of the near identical bulk SH wave velocity of PZT4 and ZnO. Finally, the transient solution oscillates near the static solution and rapidly approximates the static solution. Fig. 3 shows a comparison of transient shear stresses and static solutions when observation points are located at $(h_2/2, -h_2/2)$ within the lower layer material. This figure shows that the arrival time of transient shear stress waves satisfies physical phenomena, and the transient solution oscillates near the static solution and rapidly approximates the static solution. From the results of a comparison with the static solution and wave propagation phenomena shown in Figs. 2 and 3, we inferred that the numerical results of the double Laplace inversion calculation were correct.Below we discuss the conditions of various material thickness ratios. Fig. 4 shows the transient response of shear stresses with $h_1/h_2 = 3/2$ at an observation point of (0,0). We inferred from Fig. 4 that when $t/b_2h_2 = 1$, the incident bulk SH wave of the lower layer material reaches the observation point, when $t/b_2h_2 \cong 1.6335$, the incident bulk SH wave of the upper layer material arrives, and when $t/b_2h_2 = 3$, the first reflected wave from the free boundary ($y = -h_2$) of the lower layer material reaches the observation point. After the preliminary waves arrive and pass, the transient shear stress exhibits the phenomenon of approximating a definite value (static solution). Fig. 5 shows the transient numerical results of shear stresses with observation points at various locations. It also demonstrates that when the observation point is closer to the load, the relative transient shear stress values are all larger than when the observation point is further from the load. This indicates that when the loading distance is closer to the observation point, the induced stress value is greater. Furthermore, the arrival times of various incident, reflected, and refracted bulk SH waves

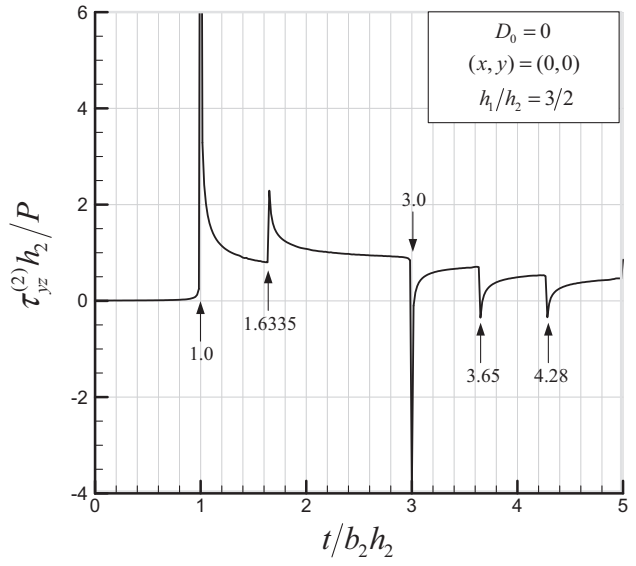

Fig. 4. Normalized transient shear stresses versus normalized time at (0,0) (N_1 = 1000, N_2 = 3000, N_3 = 3000, h_1/h_2 = 3/2, $T_t = 20b_2h_2$, αT_t = 5, T_x = 10, βT_x = 0.01.).

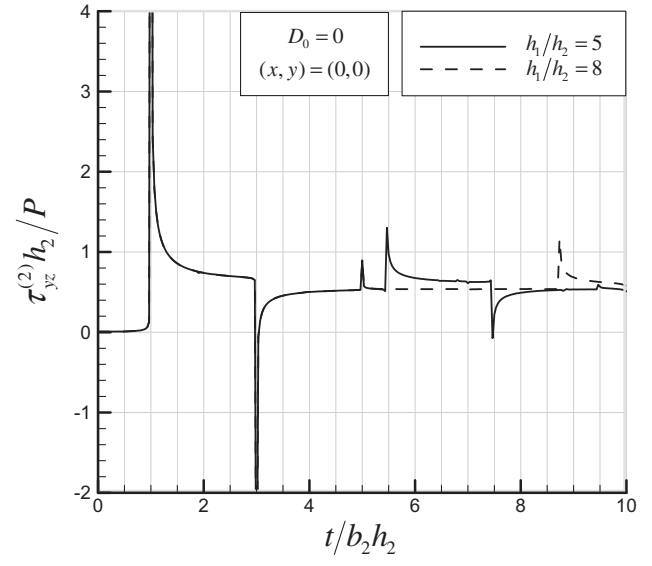

Fig. 6. Normalized transient shear stresses versus normalized time with various ratios of thickness (N_1 = 1000, N_2 = 3000, N_3 = 3000, $T_t = 20b_2h_2$, αT_t = 5, T_x = 10, βT_x = 0.01).

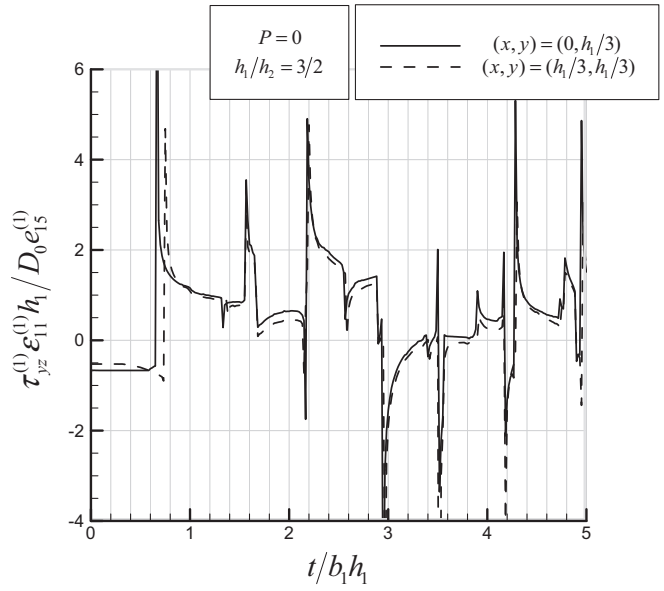

Fig. 7. Normalized transient shear stresses versus normalized time at $y = h_1/3$under electric impact only ($N_1 = 1000$, $N_2 = 3000$, $N_3 = 3000$, $h_1/h_2 = 3/2$, $T_t = 20 b_2 h_2$, $\alpha T_t = 5$, $T_x = 30$, $\beta T_x = 0.01$).

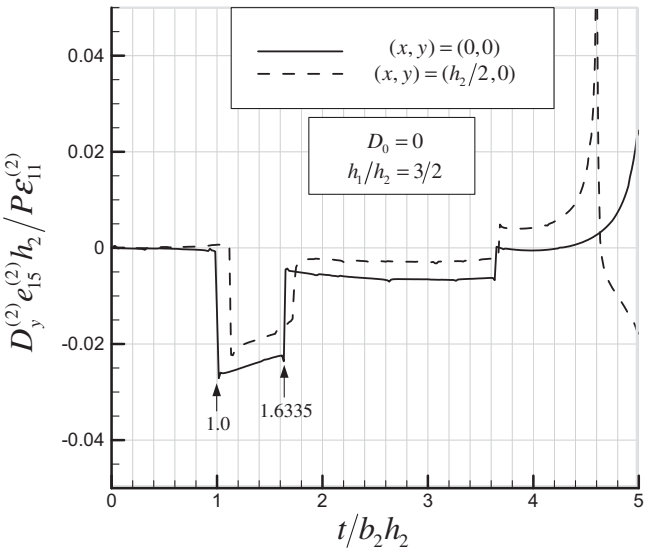

Fig. 9. Normalized transient electric displacements versus normalized time at $y = 0$ under mechanical impact only ($N_1 = 1000$, $N_2 = 3000$, $N_3 = 3000$, $h_1/h_2 = 3/2$, $T_t = 20 b_2 h_2$, $\alpha T_t = 5$, $T_x = 10$ for $(0,0)$ and $T_x = 30$ for $(h_2/2, 0)$, $\beta T_x = 0.01$).

vary with different observation points. However, they all fulfill the physical phenomena. Fig. 6 shows the transient response of shear stresses for which only a mechanical load is applied and a thickness ratio of $h_1/h_2 = 5$ and $h_1/h_2 = 8$ used. Fig. 6 shows that, because the upper layer material is significantly thicker than the lower layer material, when $t/b_2 h_2 \leqslant 5$, the waves produced are the incident bulk SH wave of the lower layer material and the related reflected waves. Therefore, the figures of $h_1/h_2 = 5$ and $h_1/h_2 = 8$ at $t/b_2 h_2 \leqslant 5$ completely overlap. However, the two figures do not separate until $t/b_2 h_2 > 5$ and the incident bulk SH wave of the $h_1/h_2 = 5$ upper layer material arrives. The accuracy of the wavefront arrival times verified that the numerical inversions in this study were correct.Fig. 7 shows the transient numerical results of shear stresses when only an electric displacement load is applied, with the observation point located at $y = h_1/3$ on the upper layer material. We can infer from Fig. 7 that based on the hypothesis that the speed of electromagnetic waves is infinite, during the beginning instant of $t = 0$, significant stress values are induced. Similarly, when the observation point is closer to the load, the values of the shear stress τ_{yz} are greater compared to the situation when the observation points are further from the load. Fig. 8 shows the transient shear stresses when various electric displacement loads are applied to the observation point $(0,0)$. Similarly, Fig. 8 shows that, electric effects induce significant stress values during the instant of $t = 0$. Furthermore, the greater the applied electric displacement load, the greater the produced shear stress.Subsequently, the transient numerical results of the electric displacement were calculated. Fig. 9 shows the transient electric displacement results when only a mechanical load is applied, with observation points in various locations. When the observation point is at $(0,0)$ and

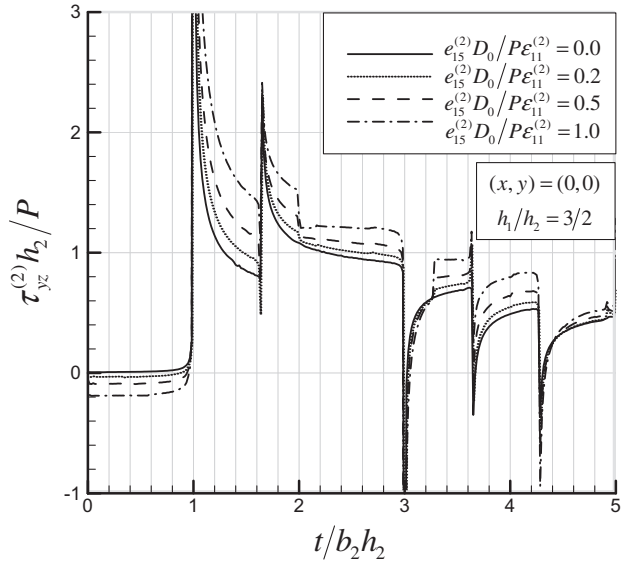

Fig. 8. Normalized transient shear stresses versus normalized time at $(0,0)$ under various electric impacts ($N_1 = 1000$, $N_2 = 3000$, $N_3 = 3000$, $h_1/h_2 = 3/2$, $T_t = 20 b_2 h_2$, $\alpha T_t = 5$, $T_x = 10$, $\beta T_x = 0.01$).

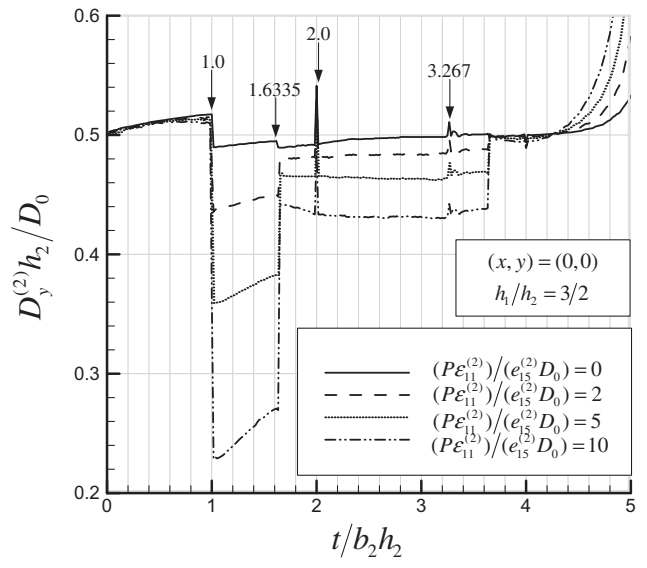

Fig. 10. Normalized transient electric displacements versus normalized time at $(0,0)$ under various mechanical impacts ($N_1 = 1000$, $N_2 = 3000$, $N_3 = 3000$, $h_1/h_2 = 3/2$, $T_t = 20 b_2 h_2$, $\alpha T_t = 5$, $T_x = 10$, $\beta T_x = 0.01$).

$t/b_1h_1 = 1$, the incident bulk SH wave from the lower layer material arrives, and when $t/b_1h_1 \cong 1.6335$, the incident bulk SH wave of the upper layer material reaches the observation point. Fig. 9 shows that the electric displacement generated by the piezoelectric material when mechanical load is applied is minor. Fig. 10 shows the transient numerical values of the electric displacement at observation point (0,0) under various mechanical and electric displacement loads. The results indicate that significant stress values are produced at $t = 0$ because of the electric effect when electric displacement is applied. When $t/b_2h_2 = 1$, the incident bulk SH wave of the lower layer material reaches the observation point, and when $t/b_2h_2 \cong 1.6335$, the incident bulk SH wave of the upper layer material reaches the observation point. In addition, the incident electromagnetic wave produced by the lower layer material instantaneously reaches the interface of the two materials, subsequently producing a reflected bulk SH wave. When $t/b_2h_2 = 2$, this reflected bulk SH wave reflects from the free surface of the lower layer material and passes through the observation point. Similarly, when $t/b_2h_2 \cong 3.267$, reflected waves reflected from the upper layer material border pass through the observation point. Greater electric displacement changes caused by the arrival of these waves are only significant and observable when mechanical and electrical displacement loads are applied simultaneously. The previous results from the application of mechanical loads alone had a minor influence on electric displacement; therefore, the changes and phenomena could not be observed.

4. Conclusions

In numerous studies, Laplace transforms have been used to solve the transient wave problems of piezoelectric materials, where accurately calculating the numerical inversion of Laplace transforms is crucial. This study successfully derived the extended Durbin method for the two-sided Laplace transform and applied the new method to the transient problem of a two-layered piezoelectric composite subjected to anti-plane mechanical and in-plane electric impacts. The results showed that the arrival time of transient shear stress waves satisfies physical phenomena, and the transient solution oscillates near the static solution and rapidly approximates the static solution. Thus, the Durbin method and the proposed extended Durbin method for Laplace transform inversions can achieve good accuracy for transient solutions. In previous studies, the Durbin method was considered to be unable to provide accurate long-term results; however, we found that simply increasing the setting for period T resolved this inefficiency. Although this change can vary the short-term results, the accuracy of the results and the calculation efficiency remain comparatively high. This study also recommended values for the time period settings of the extended Durbin method.

Acknowledgment

The authors gratefully acknowledge the financial support provided for this study by the National Science Council (Republic of China) under grant NSC 100-2221-E-032-021-MY2.

References

Abate, J., Valkó, P.P., 2004. Multi-precision Laplace transform inversion. Int. J. Numer. Methods Eng. 60, 979–993.
Albrecht, P., Honig, G., 1977. Numerical inversion of Laplace transforms: [Numerische inversion der Laplace-transformierten]. Angew. Inform. 8, 336–345.
Bellman, R.E., Kalaba, R.E., Lockett, J., 1966. Numerical Inversion of Laplace transform. American Elsevier, New York.
Cagniard, L., 1939. Reflexion et Refraction des Ondes Seismiques Progressives. Gauthiers-Villars, Paris (Translated into English and revised by Flinn, E.A., Dix, C.H., 1962. Reflection and Refraction of Progressive Seismic Waves. McGraw Hill, New York).
Chen, X., Chandra, N., Rajendran, A.M., 2004. Analytical solution to the plate impact problem of layered heterogeneous material systems. Int. J. Solids Struct. 41, 4635–4659.
Crump, K.S., 1976. Numerical inversion of Laplace transforms using a Fourier series approximation. J. Assoc. Comput. Mach. 23, 89–96.
Dubner, H., Abate, J., 1968. Numerical inversion of Laplace transforms by relating them to the finite Fourier cosine transform. J. Assoc. Comput. Mach. 15, 115–123.
Durbin, F., 1974. Numerical inversion of Laplace transforms: an efficient improvement to Dubner and Abate's method. Comput. J. 17, 371–376.
Evans, G.A., 1993. Numerical inversion of Laplace transforms using contour methods. Int. J. Comput. Math. 49, 93–105.
Gilbert, F., Backus, G.E., 1966. Propagator matrices in elastic wave and vibration problems. Geophysics 31, 326–332.
Haskell, N., 1953. The dispersion of surface waves in multilayered media. Bull. Seismol. Soc. Am. 43, 17–34.
Honig, G., Hirdes, U., 1984. A method for the numerical inversion of Laplace transforms. J. Comput. Appl. Math. 10, 113–132.
Hosono, T., 1981. Numerical inversion of Laplace transform and some applications to wave optics. Radio Sci. 16, 1015–1019.
Ing, Y.S., Liao, H.F., 2012. Investigation on transient responses of a piezoelectric crack by using Durbin and Zhao methods for numerical inversion of Laplace transforms. J. Mech. (in press).
Kundu, T., Mal, A.K., 1985. Elastic waves in a multilayered solid due to a dislocation source. Wave Motion 7, 459–471.
Kwok, Y.K., Barthez, D., 1989. An algorithm for the numerical inversion of Laplace transforms. Inverse Prob. 5, 1089–1095.
Liu, J., He, S., 2010. Properties of Love waves in layered piezoelectric structures. Int. J. Solids Struct. 47, 169–174.
Ma, C.C., Chen, X.H., Ing, Y.S., 2007. Theoretical transient analysis and wave propagation of piezoelectric bi-materials. Int. J. Solids Struct. 44, 7110–7142.
Ma, C.C., Huang, K.C., 1996. Analytical transient analysis of layered composite medium subjected to dynamic inplane impact loadings. Int. J. Solids Struct. 33, 4223–4238.
Ma, C.C., Lee, G.S., 2000. Transient elastic waves propagating in a multi-layered medium subjected to in-plane dynamic loadings. II: Numerical calculation and experimental measurement. Proc. R. Soc. Lond. A 456, 1375–1396.
Ma, C.C., Lee, G.S., 2006. General three-dimensional analysis of transient elastic waves in a multilayered medium. ASME J. Appl. Mech. 73, 490–504.
Ma, C.C., Liu, S.W., Lee, G.S., 2001. Dynamic response of a layered medium subjected to anti-plane loadings. Int. J. Solids Struct. 38, 9295–9312.
Mesquida, A.A., Otero, J.A., Ramos, R.R., Comas, F., 1998. Wave propagation in layered piezoelectric structures. J. Appl. Phys. 83, 4652–4659.
Miller, M.K., Guy, W.T., 1966. Numerical inversion of the Laplace transform by use of Jacobi polynomials. SIAM J. Numer. Anal. 3, 624–635.
Milovanović, G.V., Cvetković, A.S., 2005. Numerical inversion of the Laplace transform. Electron. Energy 18, 515–530.
Minagawa, S., 1995. Propagation of harmonic waves in a layered elasto-piezoelectric composite. Mech. Mater. 19, 165–170.
Müller, G., 1968a. Theoretical seismograms for some types of point-sources in layered media. Part I: Theory. Z. Geophys. 34, 15–35.
Müller, G., 1968b. Theoretical seismograms for some types of point-sources in layered media. Part II: Numerical calculations. Z. Geophys. 34, 147–162.
Narayanan, G.V., Beskos, D.E., 1982. Numerical operational methods for time-dependent linear problems. Int. J. Numer. Methods Eng. 18, 1829–1854.
Pao, Y.H., Gajewski, R.R., 1977. The generalized ray theory and transient responses of layered elastic solids. In: Mason, W.P., Thurston, R.N. (Eds.), Physical Acoustics, vol. 13. Academic Press, New York, pp. 183–265.
Piliposian, G.T., Avetisyan, A.S., Ghazaryan, K.B., 2012. Shear wave propagation in periodic phononic/photonic piezoelectric medium. Wave Motion 49, 125–134.
Qian, Z., Jin, F., Wang, Z., Kishimoto, K., 2004. Love waves propagation in a piezoelectric layered structure with initial stresses. Acta Mech. 171, 41–57.
Schmittroth, L.A., 1960. Numerical inversion of Laplace transforms. Commun. ACM 3, 171–173.
Sesion Jr, P.D., Albuquerque, E.L., Chesman, C., Freire, V.N., 2007. Acoustic phonon transmission spectra in piezoelectric AlN/GaN Fibonacci phononic crystals. Eur. Phys. J. B 58, 379–387.
Shih, D.H., Shen, R.C., Shiau, T.C., 1987. Numerical inversion of multidimensional Laplace transforms. Int. J. Syst. Sci. 18, 739–742.
Singhal, K., Vlach, J., Vlach, M., 1975. Numerical inversion of multidimensional Laplace transform. Proc. IEEE 63, 1627–1628.
Spencer, T.W., 1960. The method of generalized reflection and transmission coefficients. Geophysics 25, 625–641.
Spencer, T.W., 1965a. Long-time response predicted by exact elastic ray theory. Geophysics 30, 363–368.
Spencer, T.W., 1965b. Refraction along a layer. Geophysics 30, 369–388.
Therapos, C.P., Diamessis, J.E., 1982. Numerical inversion of a class of Laplace transforms. Electron. Lett. 18, 620–622.
Thomson, W.T., 1950. Transmission of elastic waves through a stratified solid. J. Appl. Phys. 21, 89–93.
Tressler, J.F., Alkoy, S., Dogan, A., Newnham, R.E., 1999. Functional composites for sensors, actuators and transducers. Compos.: Part A 30, 477–482.

Wang, S.Y., 2003. The theoretical analysis of mechanical and electric field of piezoelectric materials for multi-layered, wedge shape and circular boundary problems. Master's Thesis, National Taiwan University, ROC.

Wang, Y.Z., Li, F.M., Huang, W.H., Wang, Y.S., 2008. The propagation and localization of Rayleigh waves in disordered piezoelectric phononic crystals. J. Mech. Phys. Solids 56, 1578–1590.

Week, W.T., 1966. Numerical inversion of Laplace transforms using Laguerre functions. J. Assoc. Comput. Mach. 13, 419–429.

Wu, J.L., Chen, C.H., Chen, C.F., 2001. Numerical inversion of Laplace transform using Haar wavelet operational matrices. IEEE Trans. Circuits Syst. I: Fundam. Theory Appl. 48, 120–122.

Zakharenko, A.A., 2005. Love-type waves in layered systems consisting of two cubic piezoelectric crystals. J. Sound Vib. 285, 877–886.

Zakian, V., Coleman, R., 1971. Numerical inversion of rational Laplace transforms. Electron. Lett. 7, 777–778.

Zhao, X., 2004. An efficient approach for the numerical inversion of Laplace transform and its application in dynamic fracture analysis of a piezoelectric laminate. Int. J. Solids Struct. 41, 3653–3674.

Zhuang, S., Ravichandran, G., Grady, D.E., 2003. An experimental investigation of shock wave propagation in periodically layered composites. J. Mech. Phys. Solids 51, 245–265.